Mathematical and Computational Applications

MDPI

Article

A Modified Time-Fractional Lord–Shulman Approach to Thermoelasticity in Hollow Spheres with Variable Thermal Conductivity

Ashraf M. Zenkour [1,*], Noha M. Seyam [2] and Maryam H. Aljadani [3]

[1] Department of Mathematics, Faculty of Science, King Abdulaziz University, P.O. Box 80203, Jeddah 21589, Saudi Arabia
[2] Department of Mathematics, College of Applied Sciences, Umm Al-Qura University, P.O. Box 21955, Makkah 715, Saudi Arabia; nmseyam@uqu.edu.sa
[3] Department of Mathematics, Jamoum University College, Umm Al-Qura University, Jamoum 25375, Saudi Arabia; mhjadani@uqu.edu.sa
* Correspondence: zenkour@kau.edu.sa; Tel.: +966-540055690

Abstract

This study investigates a 2D fractional order generalized thermoelastic problem in a homogeneous and isotropic thermoelastic hollow sphere. The sphere is exposed to a decaying heat source, and the governing equations are derived using a refined fractional-order Lord–Shulman (LS) model of generalized thermoelasticity. The Laplace transform technique is used to convert time-dependent PDEs into simpler ODEs in the Laplace domain. Its numerical inversion method is used to revert to the time domain. Numerical simulations are carried out to investigate the distributions of temperature, displacement, and stress fields within the hollow sphere. The obtained results reveal that both the fractional-order parameter and the variable thermal conductivity strongly affect the thermoelastic response, particularly the propagation characteristics of thermal waves, stress intensity, and relaxation behavior. In addition, the curvature of the hollow geometry plays an important role in modifying the radial and circumferential stress distributions and their attenuation throughout the medium.

Keywords: hollow sphere; fractional-order; LS theory; decaying heat source; variable thermal conductivity

1. Introduction

The ability of a material to conduct heat under various conditions, such as temperature or spatial position (e.g., in composite or graded materials), is known as variable thermal conductivity. Several studies have explored this concept in thermoelasticity. A nonlocal thermoelastic beam model with phase lags (PLs) and variable thermal conductivity was created by Zenkour and Abouelregal [1]. The PL effects in a thermoviscoelastic orthotropic material with a cylindrical hollow under thermal shock were investigated by Zenkour and Abouelregal [2]. Mashat et al. [3] proposed generalized thermoelastic equations for an orthotropic body with a cavity, including rotation effects and PLs. Abouelregal and Zenkour [4] analyzed thermoelastic interactions in a semi-infinite medium with variable conductivity, focusing on ultrafast laser heating using nonlocal elasticity theory. Ahmed et al. [5] applied the modified extended direct algebraic approach to analyze nonlinear thermoelastic equations based on the Lord–Shulman (LS) theory, where material

Check for updates

Received: 25 April 2026
Revised: 29 May 2026
Accepted: 10 June 2026
Published: 12 June 2026

Copyright: © 2026 by the authors. Licensee MDPI, Basel, Switzerland. This article is an open access article distributed under the terms and conditions of the Creative Commons Attribution (CC BY) license.

properties and deformation vary significantly under thermal loads. Ramadan et al. [6] analytically investigated nonlinear thermoelastic behavior with internal heat sources using the Green–Naghdi (GN II) theory.

Fractional heat conduction models have been investigated in several studies, especially in spherical coordinates and with temperature-dependent thermal conductivity. A time-fractional heat conduction equation in spherical coordinates was obtained by Ning and Jiang [7]. Youssef and Abbas [8] incorporated linear temperature-dependent thermal conductivity in fractional thermoelasticity, solving 1D half-space problems. Lotfy et al. [9] considered a 1D fractional heat model for semiconductors in a spherical cavity, including magnetic field and stress effects. Lotfy [10] extended this work, analyzing temperature-dependent thermal conductivity in a semiconductor with a spherical hole. Geetanjali et al. [11] studied variable conductivity and diffusivity in a 2D half-space by means of a fractional dual-phase-lag (DPL) model. Youssef [12] developed a 3D fractional thermoelastic model with variable conductivity based on the Moore–Gibson–Thompson theorem. Hendy and Ezzat [13] investigated fractional viscoelastic piezoelectric materials with variable thermal conductivity in a medium.

Fractional calculus helps model complex thermal–mechanical behaviors. Studies cover piezoelectric rods, multi-layered plates, microplates, and porous media. Focus on dynamic thermal responses in advanced materials. Ma and He [14] studied a functionally graded (FG) piezoelectric rod under a moving heat source using fractional order thermoelasticity. Material properties varied exponentially along the road, except for a constant thermal relaxation time and specific heat. Bhoyar et al. [15] analyzed a multi-layered elliptical plate using time-fractional thermoelasticity. The plate was isotropic, homogeneous, and aligned perpendicular to the z-direction. A fractional-order thermo-viscoelastic model for small-scale effects was created by Tian et al. [16]. They used it to investigate the effects of heat stress on a viscoelastic microplate. Fractional three-phase-lag (TPL) thermoelasticity in a micropolar half-space with voids is investigated by Roy and Lahiri [17]. They used eigenvalue techniques and normal mode analysis to solve the problems.

Heat conduction and thermoelasticity in spherical geometries have been studied using fractional-order calculus. Heat absorption in a centrally symmetric sphere and the time-fractional heat equation with a Caputo derivative were examined by Povstenko and Klekot [18]. Mittal and Kulkarni [19] used a two-temperature theory to investigate fractional thermoelasticity. Shah et al. [20] used a power-law kernel in the generalized Cattaneo heat flow model to evaluate the time-fractional diffusion equation in a sphere under time-dependent Dirichlet conditions. Sheikh et al. [21] used a generalized two-temperature theory to present a coupled non-Fourier heat and non-Fick moisture diffusion model within fractional hygrothermoelasticity. Green–Lindsay (GL) generalized thermoelasticity was used by Kanoria and Ghosh [22] to study thermoelastic interactions in an FG hollow sphere with temperature-dependent characteristics.

Recent studies have advanced thermoelasticity theories using fractional-order models and unified formulations. Abo-Dahab and Abbas [23] explored transient magneto-thermoelastic phenomena with variable thermal conductivity via the LS model. Sur and Kanoria [24] industrialized a two-temperature generalized thermoelasticity theory with fractional heat conduction, unifying the 2TLS and 2TGN models. Islam and Kanoria [25] analyzed thermoelastic stress and temperature in a piezoelastic medium using fractional two-temperature theory (2TT), combining different models. Shariyat and Sedaghat [26] studied wave propagation in annular discs under mechanical/thermal loads using time-fractional LS thermoelasticity, while [27] compared integer-order (classical/LS) and fractional-order thermo-viscoelastic responses. Zenkour et al. [28] adopted fractional-order refined LS

theory to model skin tissue under ramp heating, evaluating classical, LS, and refined LS models.

Several studies have explored heat conduction and thermoelastic behavior in spheres and nanobeams using non-Fourier and generalized thermoelasticity theories. Babaei and Chen [29] examined hyperbolic heat conduction in a heterogeneous sphere with radially varying material properties (power law) and constant thermal relaxation time. Zenkour et al. [30] modeled nonlocal thermoelastic vibrations of an Euler–Bernoulli nanobeam using the LS theory (one relaxation time). Abbas [31] derived exact solutions for free vibrations of a thermoelastic hollow sphere using LS theory with eigenvalue approaches. Mishra and Sharma [32] studied radial vibrations of an FG thermoelastic hollow sphere under thermal load (LS model), with properties varying radially via a power law. Jani et al. [33] examined a piezoelectric hollow sphere under sudden thermal shock, assuming symmetric loading and boundary conditions. Branco et al. [34] revisited heat conduction in an insulated sphere with dimensionless analysis, accounting for convection-dependent heat transfer coefficients. Kar and Kanoria [35] analyzed thermoelastic interactions in a spherical shell subjected to a temperature step input, solving governing equations via Laplace transforms and eigenvalue methods. Ghosh and Kanoria [36] investigated displacements/stresses in an FG hollow sphere (GL theory, two relaxation times). Sharma et al. [37] considered free vibrations of a porous thermoelastic hollow sphere under DPL thermoelasticity and nonlocal elasticity. Sharma et al. [38] modeled transient vibrations in a hollow sphere with diffusion and nonlocal elasticity, subjected to harmonic heat sources (stress-free, isothermal boundaries).

We compared this with analytical benchmarks to validate the fractional model's accuracy. This analysis highlights the importance of fractional calculus in capturing complex deformation behaviors in thermoelastic materials. This research examines a 2D fractional-order thermoelastic problem in a homogeneous, isotropic hollow sphere under a decaying heat source. The fractional LS framework extends generalized thermoelasticity by introducing memory-dependent thermal relaxation, which enables the model to capture experimentally observed phenomena such as finite-speed thermal wave propagation, attenuation, and stress-relaxation effects under transient heating. The governing equations are based on a fractional-order LS model. Laplace transforms convert time-dependent PDEs into simpler ODEs. A numerical inversion method retrieves time-domain solutions. Displacement, temperature, and stress distributions are computed and visualized. The fractional-order parameter and variable thermal conductivity significantly influence thermoelastic fields. The decaying heat source causes transient thermal stresses, with the fractional parameter affecting peak stresses and relaxation times. Curvature effects impact radial and hoop stresses, while the fractional order alters their spatial decay. From a computational perspective, the fractional LS model provides a smooth and controllable transition between classical and generalized behaviors through the fractional order, allowing improved fitting to experimental data without increasing model complexity or introducing additional internal variables. Relevant references have been added to support the physical and computational advantages of fractional formulation.

The organization of the paper is as follows. Section 1 presents the introduction and the background of the problem. Section 2 introduces the fundamental governing equations, including the time-fractional heat conduction equation, Cauchy relations, equations of motion, constitutive relations, variable thermal conductivity, as well as the corresponding boundary and initial conditions. Section 3 is devoted to the analytical solution of the problem using the Laplace transform technique, dimensionless physical variables, integration parameters, and the numerical inversion of the Laplace transform. Section 4 discusses the obtained numerical results and applications, including comparisons between classical

and generalized thermoelastic theories, and the effects of the fractional-order parameter, thermal conductivity parameter, and decaying heat source parameter on the thermoelastic fields. Finally, Section 5 summarizes the main conclusions and significant findings of the study.

2. Refined Fractional Order Model

Below is a summary of the constitutive and fundamental equations for a homogeneous, isotropic, annular sphere under the fractional-order theory of generalized thermoelasticity. Because of spherical symmetry, only the radial displacement $u_r = u(r,\ t)$ is non-zero when the problem is expressed in spherical coordinates (r,θ,ϕ).

2.1. Time-Fractional Heat Conduction Equation

The generalized thermal conduction equation under the refined fractional Lord–Shulman (F-LS (r)) theory is given by [39–44]

$$\mathcal{D}_1[\kappa(\Theta)\mathcal{D}_0\Theta] = \mathcal{D}[\mathcal{D}_t(\rho c_v\Theta + \gamma T_0 e) - Q], \tag{1}$$

where $\mathcal{D}_0$, $\mathcal{D}_1$, and $\mathcal{D}_t$ represent the following differential parameters:

$$\mathcal{D}_0 = \frac{\partial}{\partial r}, \mathcal{D}_1 = \frac{\partial}{\partial r} + \frac{2}{r}, \mathcal{D}_t = \frac{\partial}{\partial t}, \mathcal{D}_1\mathcal{D}_0 = \frac{\partial^2}{\partial r^2} + \frac{2}{r}\frac{\partial}{\partial r} = \nabla^2, \mathcal{D}_0\mathcal{D}_1 = \nabla^2 - \frac{2}{r^2}, \tag{2}$$

and $\mathcal{D}$ is the fractional differential parameter

$$\mathcal{D} = 1 + \sum_{n=1}^{N} \frac{\tau^{n+\beta}}{(n+\beta)!}\mathcal{D}_t^{(n+\beta)}, \mathcal{D}_t^{(n+\beta)} = \frac{\partial^{n+\beta}}{\partial t^{n+\beta}}, N \geq 1. \tag{3}$$

(i) Simple fractional derivative (FD (s)) theory (neglecting the summation):

$$\mathcal{D}_1[\kappa(\Theta)\mathcal{D}_0\Theta] = \left(1 + \frac{\tau^\beta}{\alpha!}\mathcal{D}_t^{(\beta)}\right)[\mathcal{D}_t(\rho c_v\Theta + \gamma T_0 e) - Q], 0 < \beta \leq 1. \tag{4}$$

(ii) Simple Lord–Shulman (LS (s)) theory ($\beta = 1$) :

$$\mathcal{D}_1[\kappa(\Theta)\mathcal{D}_0\Theta] = (1 + \tau\mathcal{D}_t)[\mathcal{D}_t(\rho c_v\Theta + \gamma T_0 e) - Q]. \tag{5}$$

(iii) Classical thermoelasticity (CTE) theory ($\tau = 0$) :

$$\mathcal{D}_1[\kappa(\Theta)\mathcal{D}_0\Theta] = \mathcal{D}_t(\rho c_v\Theta + \gamma T_0 e) - Q. \tag{6}$$

(iv) Refined Lord–Shulman (LS (r)) theory ($\beta \longrightarrow 0$ in Equation (1) or $\beta \longrightarrow 1$ in Equation (4)):

$$\mathcal{D}_1[\kappa(\Theta)\mathcal{D}_0\Theta] = \left(1 + \sum_{n=1}^{N} \frac{\tau^n}{n!}\mathcal{D}_t^{(n)}\right)[\mathcal{D}_t(\rho c_v\Theta + \gamma T_0 e) - Q], N \geq 1. \tag{7}$$

(v) Simple fractional Lord–Shulman (F-LS (s)) theory ($N = 1$ in Equation (1), single-term expansion):

$$\mathcal{D}_1[\kappa(\Theta)\mathcal{D}_0\Theta] = \left(1 + \frac{\tau^{1+\beta}}{(1+\beta)!}\mathcal{D}_t^{(1+\beta)}\right)[\mathcal{D}_t(\rho c_v\Theta + \gamma T_0 e) - Q], 0 < \beta \leq 1. \tag{8}$$

2.2. Cauchy Relations

The thickness and density of the annular sphere have no bearing on the relationship between stresses and the radial displacement u. The strain components and dilatation in spherical coordinates (r, θ, ϕ) are as follows:

$$e_r = \frac{\partial u}{\partial r}, \quad e_\theta = e_\phi = \frac{u}{r}, \tag{9}$$

$$e = e_r + e_\theta + e_\phi = \mathcal{D}_1 u. \tag{10}$$

2.3. Equation of Motion and Constitutive Equations

The equation of motion of the spherical system (derived from momentum balance) is

$$(\lambda + 2\mu)\mathcal{D}_0\mathcal{D}_1 u - \gamma\mathcal{D}_0\Theta = \rho\mathcal{D}_t^{(2)} u. \tag{11}$$

Also, the constitutive equations are specified by

$$\sigma_r = (\lambda + 2\mu)\mathcal{D}_0 u + \lambda\frac{2u}{r} - \gamma\Theta, \sigma_\theta = \sigma_\phi = (\lambda + 2\mu)\frac{u}{r} + \lambda\left(\mathcal{D}_0 u + \frac{u}{r}\right) - \gamma\Theta. \tag{12}$$

2.4. Variable Thermal Conductivity

The treatment of variable thermal conductivity in the context of heat conduction will be discussed by using a temperature-mapping approach. The mapping is defined as

$$\vartheta = \frac{1}{\kappa_0}\int_0^\Theta \kappa(\Theta')\mathrm{d}\Theta'. \tag{13}$$

Differentiating the mapping for time, one gets

$$\kappa_0\mathcal{D}_t\vartheta = \kappa(\Theta)\mathcal{D}_t\Theta. \tag{14}$$

Applying the spatial operator $\mathcal{D}_0$ to Equation (13) yields

$$\kappa_0\mathcal{D}_0\vartheta = \kappa(\Theta)\mathcal{D}_0\Theta. \tag{15}$$

Additionally, using the operator $\mathcal{D}_1$ on both sides of Equation (15) results in

$$\kappa_0\nabla^2\vartheta = \mathcal{D}_1[\kappa(\Theta)\mathcal{D}_0\Theta]. \tag{16}$$

This relates the Laplacian of ϑ to the divergence of the heat flux. So, the heat conduction equation that appeared in Equation (1) while neglecting the heat source becomes

$$\nabla^2\vartheta = \overline{\mathcal{D}}\left(\frac{1}{\eta}\vartheta + \frac{\gamma T_0}{\kappa_0}e\right), \quad \overline{\mathcal{D}} = \mathcal{D}\mathcal{D}_t. \tag{17}$$

The thermal conductivity as a function of temperature will now be expressed in linear form as follows:

$$\kappa(\Theta) = \kappa_0(1 + \kappa_1\Theta). \tag{18}$$

From Equations (14) and (16), one gets

$$\vartheta = \Theta + \frac{\kappa_1}{2}\Theta^2, \quad \mathcal{D}_0\vartheta = (1 + \kappa_1\Theta)\mathcal{D}_0\Theta. \tag{19}$$

The first part of Equation (19) yields

$$\Theta = \frac{-1 + \sqrt{1 + 2\kappa_1\vartheta}}{\kappa_1}. \tag{20}$$

https://doi.org/10.3390/mca31030105

2.5. Boundary and Initial Circumstances

To explain the problem's imposed beginning and boundary conditions, let us look at a few relations. The starting conditions ought to be stated as

$$\vartheta(r,0) = \frac{\partial^n}{\partial t^n}\vartheta(r,0) = 0, \quad u(r,0) = \frac{\partial^n}{\partial t^n}u(r,0) = 0, \quad n = 1,\ 2,\ 3,\ \ldots. \tag{21}$$

The annular sphere's inner and outer surfaces are both clamped; the outside surface experiences an exponential decline of temperature mapping over time, while the inner surface is isolated. These requirements are stated as

$$u(a,t) = 0, \quad u(b,t) = 0, \quad \left.\frac{\partial\vartheta(r,t)}{\partial r}\right|_{r=a} = 0, \quad \vartheta(b,t) = \vartheta_0 \mathrm{e}^{-\omega t}. \tag{22}$$

3. Solution to the Problem

3.1. The Laplace Transformation

Let us use the well-known Laplace transform provided by

$$\mathcal{L}\{f(r,t)\} = \overline{f}(r,s) = \int_0^\infty f(r,t)\, e^{-st}\mathrm{d}t. \tag{23}$$

3.2. Dimensionless Physical Variables

The dimensionless variables look like this

$$\begin{gathered}\{r',u'\} = \frac{c_0}{\eta}\{r,u\}, \quad \{t',\tau'\} = \frac{c_0^2}{\eta}\{t,\tau\}, \quad \{\Theta',\vartheta'\} = \frac{1}{T_0}\{\Theta,\vartheta\}, \quad \omega' = \frac{\eta}{c_0^2}\omega, \\ \sigma_j' = \frac{\sigma_j}{\lambda+2\mu}, \quad \kappa_1' = T_0\kappa_1, \quad c_0^2 = \frac{\lambda+2\mu}{\rho}.\end{gathered} \tag{24}$$

The thermal conductivity can be linearized as $\kappa(\Theta) \approx \kappa(T_0)$, i.e., treated as a constant at the reference temperature T_0, without losing generality. The governing expressions simplify to the following forms (primes deleted) when Equation (24) and the Laplace transform are used

$$\overline{\sigma}_r = \left(\mathcal{D}_0 + \frac{2c_1}{r}\right)\overline{u} - c_2\overline{\Theta}, \quad \overline{\sigma}_\theta = \overline{\sigma}_\phi = \left(c_1\mathcal{D}_0 + \frac{1+c_1}{r}\right)\overline{u} - c_2\overline{\Theta}, \tag{25}$$

$$(\mathcal{D}_0\mathcal{D}_1 - 2c_3)\overline{u} = c_4\mathcal{D}_0\overline{\vartheta}, \tag{26}$$

$$(\mathcal{D}_1\mathcal{D}_0 - 2c_5)\overline{\vartheta} = 2c_6\mathcal{D}_1\overline{u}, \tag{27}$$

where

$$c_1 = \frac{\lambda}{\lambda+2\mu}, \ c_2 = \frac{\gamma T_0}{\lambda+2\mu}, \ c_3 = \frac{s^2}{2}, \ c_4 = \frac{\gamma T_0}{\rho c_0^2(1+\kappa_1)}, \ c_5 = \frac{\varpi}{2}, \ c_6 = \frac{\gamma\varpi(1+\kappa_1)}{2\rho c_v}. \tag{28}$$

The theory will determine the value of the parameter ϖ. That is

(i) CTE theory:

$$\varpi = s. \tag{29}$$

(ii) The LS (s) theory:

$$\varpi = s(1+\tau\, s). \tag{30}$$

(iii) The LS (r) theory:

$$\varpi = s\left(1 + \sum_{n=1}^{N} \frac{\tau^n}{n!} s^n\right). \tag{31}$$

The Laplace transform of fractional-order models is as follows if $\beta > 0$ and $m = [\beta] + 1$ with $h(t)$, and its derivatives up to order $(m-1)$ are continuous and of exponential order on $[0, \infty)$, and its Caputo derivative is piecewise continuous:

$$\mathcal{L}\left\{\frac{\partial^\beta}{\partial t^\beta} h(t)\right\} = s^\beta \mathcal{L}\{h(t)\} - \sum_{k=0}^{m-1} s^{\beta-k-1} h^{(k)}(0). \tag{32}$$

Due to the aforementioned equation and the beginning circumstances found in Equation (21), we obtain the parameter ϖ using the fraction theory in the following form:

(iv) The FD (s) theory:

$$\varpi = s\left(1 + \frac{\tau^\beta}{\beta!} s^\beta\right). \tag{33}$$

(v) The F-LS (s) theory:

$$\varpi = s\left(1 + \frac{\tau^{1+\beta}}{(1+\beta)!} s^{1+\beta}\right). \tag{34}$$

(vi) The LS (r) theory:

$$\varpi = s\left(1 + \sum_{n=1}^{N} \frac{\tau^{n+\beta}}{(n+\beta)!} s^{n+\beta}\right), N > 1. \tag{35}$$

The physical quantities in the Laplace domain can be written as

$$\overline{\vartheta}(r) = \frac{1}{r} \sum_{j=1}^{2} \left(A_j \mathrm{e}^{\xi_j r} + B_j \mathrm{e}^{-\xi_j r}\right), \tag{36}$$

$$\overline{u}(r) = \frac{1}{r} \sum_{j=1}^{2} \eta_j \left[A_j \left(\frac{1}{r} - \xi_j\right) \mathrm{e}^{\xi_j r} + \left(\frac{1}{r} + \xi_j\right) B_j \mathrm{e}^{-\xi_j r}\right], \tag{37}$$

where A_j and B_j $(j = 1, 2)$ are the integration parameters, and

$$\xi_{1,2}^2 = c_4 c_6 + c_3 + c_5 \pm \xi_0, \eta_{1,2} = \frac{c_4 c_6 - c_3 + c_5 \mp \xi_0}{4 c_3 c_6}, \xi_0^2 = (c_4 c_6 + c_3 + c_5)^2 - 4 c_3 c_5. \tag{38}$$

The temperature of the hollow sphere in the Laplace domain may be obtained as

$$\overline{\Theta}(r) = \frac{1}{\kappa_1} \left\{\left[1 + \frac{2\kappa_1}{r} \sum_{j=1}^{2} \left(A_j \mathrm{e}^{\xi_j r} + B_j \mathrm{e}^{-\xi_j r}\right)\right]^{1/2} - 1\right\}. \tag{39}$$

The stresses may be found in the Laplace domain as

$$\{\overline{\sigma}_r, \overline{\sigma}_\theta\} = -\frac{1}{r} \sum_{j=1}^{2} \left(\{\hat{\zeta}_j, \hat{\chi}_j\} A_j \mathrm{e}^{\xi_j r} + \{\check{\zeta}_j, \check{\chi}_j\} B_j \mathrm{e}^{-\xi_j r}\right) - c_2 \overline{\Theta}(r), \tag{40}$$

where

$$\hat{\zeta}_j, \check{\zeta}_j = \eta_j \left[\xi_j^2 \pm \frac{2}{r}(c_1 - 1)\left(\xi_j \mp \frac{1}{r}\right)\right], \hat{\chi}_j, \check{\chi}_j = \eta_j \left[c_1 \xi_j^2 \mp \frac{1}{r}(2c_1 - c_2 - 1)\left(\xi_j \mp \frac{1}{r}\right)\right]. \tag{41}$$

https://doi.org/10.3390/mca31030105

It is interesting to get the dilatation in Equation (10) with the aid of the above solutions in the form

$$\bar{e}(r) = -\frac{1}{r}\sum_{j=1}^{2} \eta_j \xi_j^2 \left(A_j \mathrm{e}^{\xi_j r} + B_j \mathrm{e}^{-\xi_j r} \right). \tag{42}$$

3.3. Integration Parameters

The Laplace transform domain boundary conditions (22) are as follows:

$$\overline{u}(a,s) = \overline{u}(b,s) = 0, \overline{\vartheta}(a,s) = 0, \overline{\vartheta}(b,s) = \overline{G}(s) = \frac{\vartheta_0}{s+\omega}. \tag{43}$$

The following simultaneous equations will provide the parameters A_j, B_j, j =1, 2 under the aforementioned conditions

$$\begin{bmatrix} \eta_1\left(\frac{1}{a}-\xi_1\right) & \eta_2\left(\frac{1}{a}-\xi_2\right) & \eta_1\left(\frac{1}{a}+\xi_1\right) & \eta_2\left(\frac{1}{a}+\xi_2\right) \\ \eta_1\left(\frac{1}{b}-\xi_1\right) & \eta_2\left(\frac{1}{b}-\xi_2\right) & \eta_1\left(\frac{1}{b}+\xi_1\right) & \eta_2\left(\frac{1}{b}+\xi_2\right) \\ \frac{1}{a}-\xi_1 & \frac{1}{a}-\xi_2 & \frac{1}{a}+\xi_1 & \frac{1}{a}+\xi_2 \\ 1 & 1 & 1 & 1 \end{bmatrix} \begin{Bmatrix} A_1 \\ A_2 \\ B_1 \\ B_2 \end{Bmatrix} = \begin{Bmatrix} 0 \\ 0 \\ 0 \\ b\,G(s) \end{Bmatrix}. \tag{44}$$

All the annular sphere's field quantities in the Laplace domain are determined by the parameters A_j and B_j, which are obtained by solving the system.

3.4. Numerical Inversion of the Laplace Transform

A numerical methodology based on the Riemann sum method is obtained by inverting the transform [45,46]. The Laplace transform of $f(r,t)$ for fixed r is $\overline{f}(r,s)$, while the inverse $f(r,t)$ is roughly represented by:

$$f(r,t) = \frac{\mathrm{e}^{ct}}{t}\left[\frac{1}{2}\overline{f}(r,c) + \mathrm{Re}\left(\sum_{m=1}^{M}(-1)^m \overline{f}\left(r,\ c+\frac{\rangle m\pi}{t}\right)\right)\right]. \tag{45}$$

Numerical studies indicate that $ct \approx 4.7$ for faster convergence [45,46]. It is fixed at $M = 50$ for all results presented in the manuscript, ensuring high accuracy. All formulas are then converted into the Laplace domain using a numerical algorithm.

4. Discussions and Applications

This work provides a fractional-order thermoelastic framework for analyzing transient thermal–mechanical interactions in hollow spheres. The findings demonstrate how fractional calculus may be used to forecast thermal stresses and wave propagation, offering valuable information for material design under thermal loads. Applications to evaluate the effects of various models will be investigated in future work. The components of the hollow sphere are roughly represented by:

$$\begin{gathered} \lambda = 7.76 \times 10^{10}\ \mathrm{N\,m^{-2}}, \quad \mu = 3.86 \times 10^{10}\ \mathrm{N\,m^{-2}}, \quad \kappa_0 = 386\ \mathrm{W\,m^{-1}\,K^{-1}}, \\ \rho = 8954\ \mathrm{kg\,m^{-3}}, \quad \alpha_t = 1.78 \times 10^{-5}\ \mathrm{K^{-1}}, \quad c_v = 383.1\ \mathrm{J\,kg^{-1}\,K^{-1}}, \quad T_0 = 293\ \mathrm{K}. \end{gathered} \tag{46}$$

Scaled real values of the thermoelastic variables are utilized for ease of usage. These results are calculated for $t = 0.3$, $\tau = 0.02$, and $\phi_0 = 100$. Unless otherwise noted, some parameters have fixed values, such as $\omega = 10$, and $\kappa_0 = 1.1$. The temperature-mapping $\breve{\vartheta} \equiv 10^{-1} \times \vartheta(r,t)$, temperature $\breve{\theta} \equiv 10^{-1} \times \theta(r,t)$, radial displacement $\breve{u} \equiv 10^{3} \times u(r,t)$, dilatation $\breve{e} \equiv 10^{2} \times e(r,t)$, radial stress $\breve{\sigma}_r \equiv 10 \times \sigma_r(r,t)$, and hoop stress $\breve{\sigma}_\theta \equiv 10 \times \sigma_\theta(r,t)$ as a result of the different theories under consideration. Figures 1–23 show the results.

4.1. Comparison Between Classical and Generalized Thermoelastic Theories

Figure 1 consists of two plots to compare different generalized theories for solving the temperature-mapping problem $\breve{\vartheta}$ as a function of the radial direction of the sphere r, under two conditions for the fractional parameter β. In Figure 1a, the refined fractional F-LS (r) theory shows high-frequency oscillations with sharp peaks and troughs, indicating sensitivity or high-order accuracy in this coordinate system. The F-LS (s) and FD (s) theories are smoother but deviate from the F-LS (r) theory, especially in regions of higher variation ($r > 0.7$). All fractional theories converge at the boundaries near $r = 1$. In Figure 1b, the curve of $\breve{\vartheta}$ due to the LS (r) theory showing oscillations, but less dramatic than in Figure 1a, indicating the absence of β smooths in the temperature-mapping $\breve{\vartheta}$. All theories closely follow each other from $r = 0.2$ to $r \approx 0.7$, diverging slightly afterward. The CTE and LS (s) theories align well, suggesting strong agreement in smoother regions.

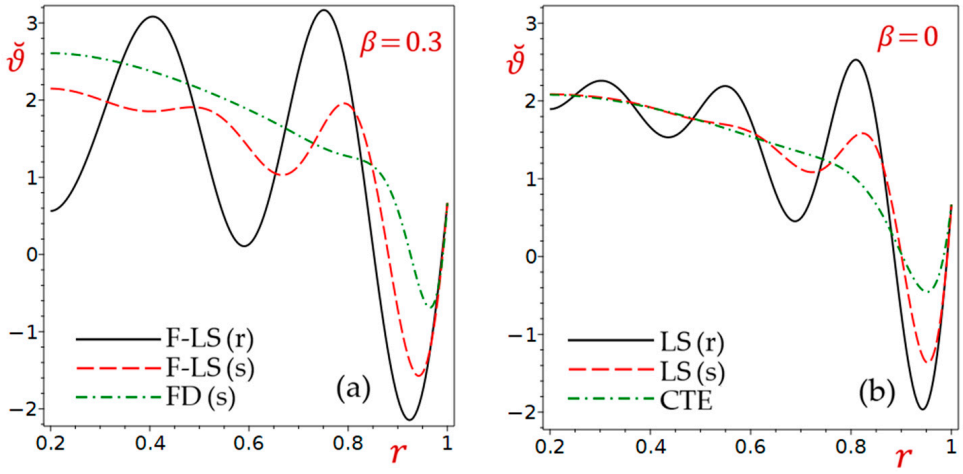


Figure 1. The temperature-mapping $\breve{\vartheta}$ of the hollow sphere with and without the fraction parameter (**a**) $\beta = 0.3$ (**b**) $\beta = 0$.

Figure 2 consists of two plots of temperature $\breve{\Theta}$ comparing different theories or conditions for a parameter β set to 0.3 and 0, respectively. Figure 2a shows the temperature distribution $\breve{\Theta}$ for a hollow sphere with a fractional parameter $\beta = 0.3$. Three curves are plotted to exhibit distinct behaviors, suggesting that the choice of theory (simple and refined F-LS vs. FD) significantly impacts the temperature profile. The temperature distribution is smooth, indicating the influence of the fractional parameter $\beta = 0.3$ on the temperature's regularity. Figure 2b displays the temperature distribution $\breve{\Theta}$ for the case where the fractional parameter $\beta = 0$. The temperature values are negative, which might indicate a normalized or relative temperature scale. The curves diverge as r increases, highlighting the impact of the domain or boundary conditions when $\beta = 0$. The absence of the fractional parameter leads to sharper transitions or less smooth behavior compared to Figure 2a.

The radial displacement $\breve{u}$ for (a) $\beta = 0.3$ and (b) $\beta = 0$ is shown in Figure 3. Every curve in Figure 3a shows nonlinear degradation as r increases. The FD (s) curve has a small deviation, suggesting the impact of the fractional parameter, although the F-LS (r) and F-LS (s) findings are almost identical. The displacement is less negative in Figure 3b, indicating the function of β. While the CTE model displays a greater decline, the LS (r) and LS (s) curves overlap. Overall, adding $\beta = 0.3$ results in greater inward displacements, indicating that fractional models, both simple and refined, predict stronger deformation than classical and generalized theories.

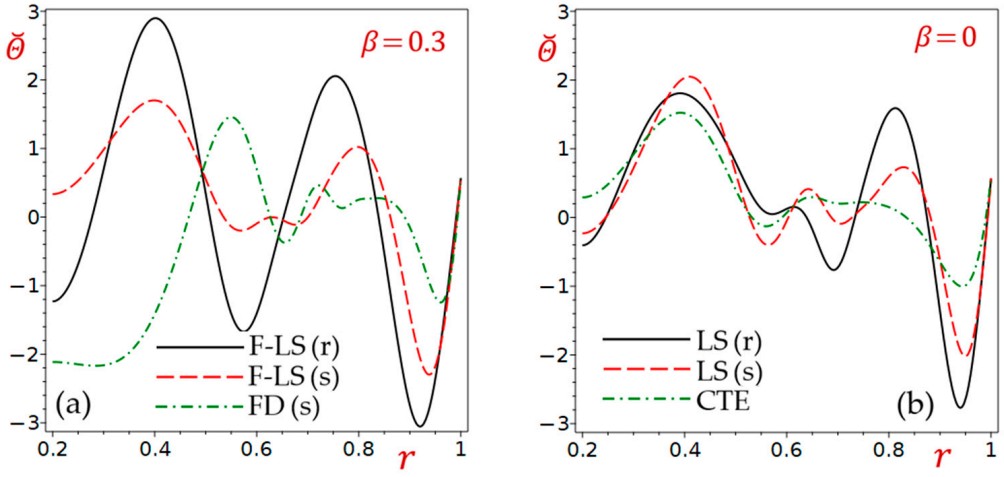


Figure 2. The temperature $\breve{\Theta}$ of the hollow sphere with and without the fraction parameter (**a**) $\beta = 0.3$ (**b**) $\beta = 0$.

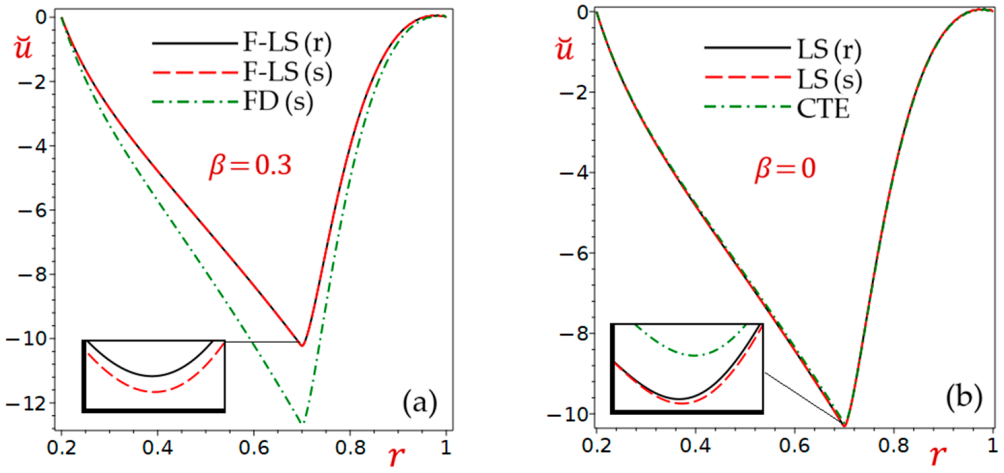


Figure 3. The radial displacement $\breve{u}$ of the hollow sphere with and without the fraction parameter (**a**) $\beta = 0.3$ (**b**) $\beta = 0$.

Figure 4 displays the dilatation $\breve{e}$ for (a) $\beta = 0.3$ and (b) $\beta = 0$. All the curves in Figure 4a begin close to $\breve{e} \approx -4$ and diverge as r increases. While F-LS (r) and F-LS (s) display comparable but less noticeable tendencies, the FD (s) model has the highest compression. This suggests that compressive effects are enhanced by the fractional parameter, with slightly higher deformation predicted by revised models. LS (r) and LS (s) almost coincide in Figure 4b, but CTE deviates somewhat. The models converge when fractional effects are absent, indicating a decrease in the discrepancies between generalized and classical theories.

The radial stress $\breve{\sigma}_r$ for (a) $\beta = 0.3$ and (b) $\beta = 0$ is compared in Figure 5. The stress exhibits alternating increases and decreases along r in Figure 5a. The FD (s) model produces the lowest results, the improved F-LS (r) model produces the highest, and F-LS (s) falls in the middle. Reduced fractional influence is indicated by the convergence of the curves as $r \to 1$. A similar pattern can be seen in Figure 5b, although the differences are less pronounced. While LS (s) and CTE almost coincide, suggesting that the reaction approaches classical behavior in the absence of fractional effects, the refined LS (r) predicts slightly higher stress.

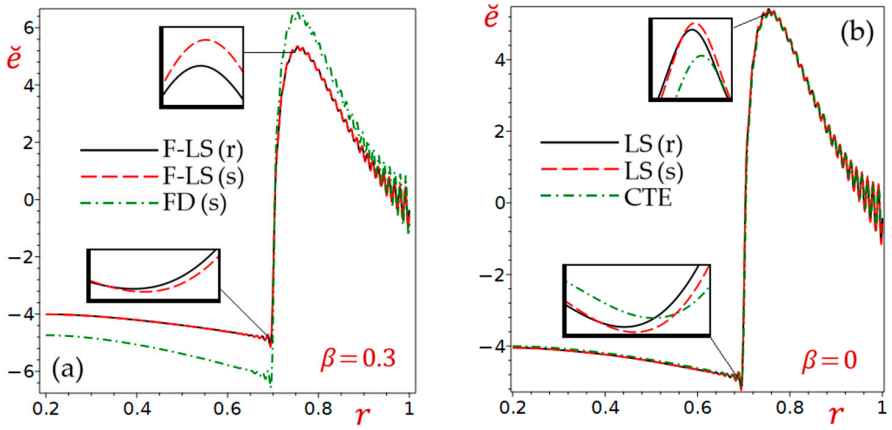


Figure 4. The dilatation $\breve{e}$ of the hollow sphere with and without the fraction parameter (**a**) $\beta = 0.3$ (**b**) $\beta = 0$.

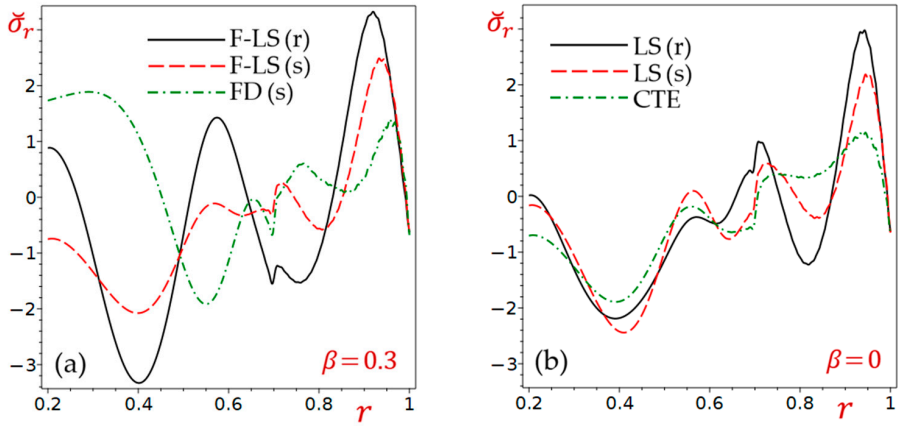


Figure 5. The radial stress $\breve{\sigma}_r$ of the hollow sphere with and without the fraction parameter (**a**) $\beta = 0.3$ (**b**) $\beta = 0$.

The hoop stress $\breve{\sigma}_\theta$ for (a) $\beta = 0.3$ and (b) $\beta = 0$ is compared in Figure 6. The fractional models exhibit discernible change with r in Figure 6a. While F-LS (s) and FD (s) are simpler, the refined F-LS (r) displays smoother and more sophisticated behavior. The stress exhibits significant fluctuations because of fractional effects, ranging from compressive to tensile values. The curves get closer and smoother in Figure 6b. While LS (s) and CTE almost overlap, LS (r) exhibits somewhat richer dynamics. It is confirmed that fractional effects improve stress variation and model sensitivity when β is absent.

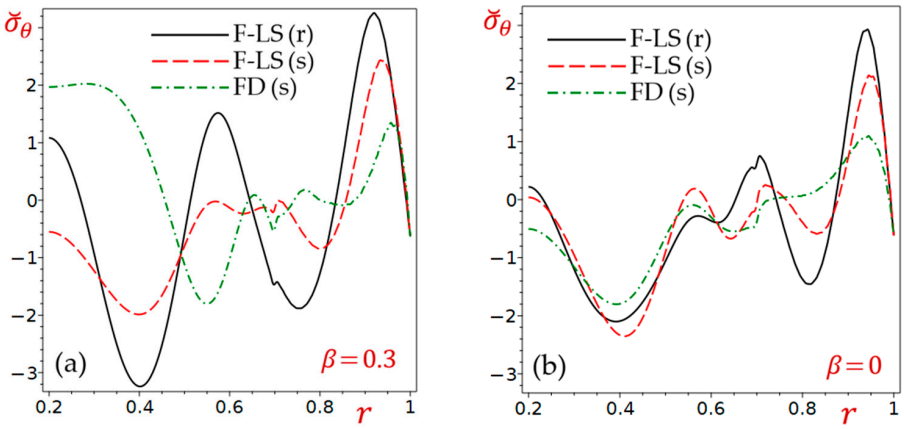


Figure 6. The hoop stress $\breve{\sigma}_\theta$ of the hollow sphere with and without the fraction parameter (**a**) $\beta = 0.3$ (**b**) $\beta = 0$.

4.2. Effect of Fractional Parameter β

Figure 7 illustrates how the fractional parameter β influences the temperature-mapping distribution $\breve{\vartheta}$ in the hollow sphere under the refined F-LS (r) model. It shows curves for three values of β: 0.5, 0.2, and 0. For $\beta = 0$ (weaker fractional effect), the temperature distribution might exhibit the most gradual or smoothed variation, suggesting significant memory or non-local damping of thermal waves. For $\beta = 0.5$ (strongest fractional effect), the temperature-mapping gradient could be steeper, indicating a more localized or classical-like thermal response. The curve for $\beta = 0.2$ lies between the other two, showing an intermediate behavior. The figure highlights the sensitivity of thermal modeling to the fractional parameter β, emphasizing the importance of choosing β appropriately to match experimental or observed thermal behavior in materials with memory or non-local effects.

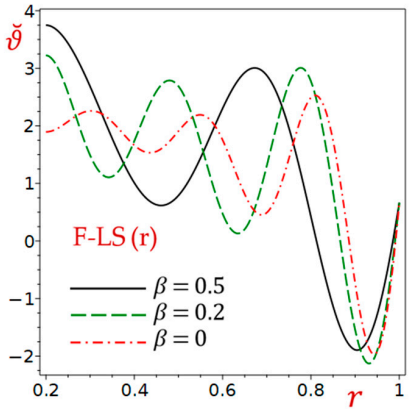


Figure 7. Effect of fractional parameter β on temperature-mapping $\breve{\vartheta}$ of the hollow sphere due to the refined F-LS (r) theory.

Figure 8 illustrates the effect of the fractional parameter β on the temperature $\breve{\Theta}$ of a hollow sphere under the refined fractional Lord and Shulman (F-LS (r)) theory. The graph shows three distinct curves corresponding to different values of β. All curves exhibit a similar pattern, but their amplitudes and rates of change vary with β. As β decreases (from 0.5 to 0), the temperature distribution appears to become more pronounced or sharper, indicating a stronger thermal response or faster thermal diffusion for smaller β values. The curve for $\beta = 0.5$ shows a moderate thermal response, suggesting a balanced influence of fractional effects. For $\beta = 0.2$ the curve exhibits a steeper or more exaggerated response compared to $\beta = 0.5$, implying enhanced thermal effects as β reduces. The curve due to $\beta = 0$ represents the limiting case where the fractional effect is minimized or absent, leading to the most distinct temperature profile, possibly aligning with classical theory predictions.

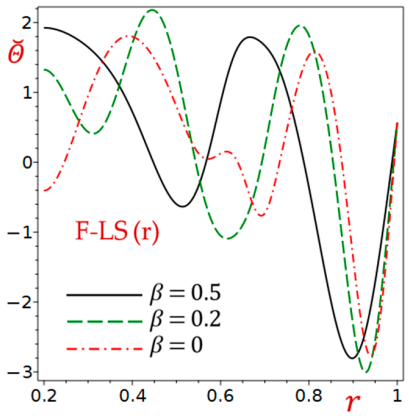


Figure 8. Effect of fractional parameter β on temperature $\breve{\Theta}$ of the hollow sphere due to the refined F-LS (r) theory.

Figure 9 illustrates the effect of the fractional parameter β on the radial displacement $\breve{u}$ of the hollow sphere, as analyzed using the refined fractional Lord and Shulman (F-LS (r)) theory. The graph plots $\breve{u}$ against the radial direction r, with r ranging from 0.2 to 1. Three distinct curves are shown, each corresponding to a different value of β. For all values of β, the radial displacement $\breve{u}$ is negative, indicating inward displacement (toward the center of the sphere). The magnitude of $\breve{u}$ decreases (becomes less negative) as r increases, suggesting that $r \approx 0.7$ reduces the inward displacement. The curve of $\breve{u}$ for $\beta = 0.5$ (solid line) shows the least negative displacement, followed by $\beta = 0.2$ (dashed line), and $\beta = 0$ (dotted line) exhibits the most negative displacement. This implies that as β increases, the inward radial displacement becomes more pronounced. The fractional parameter β significantly influences the mechanical response of the hollow sphere, with higher β values leading to greater deformation.

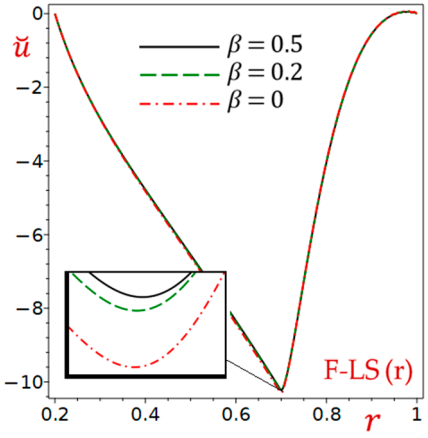


Figure 9. Effect of fractional parameter β on radial displacement $\breve{u}$ of the hollow sphere due to the refined F-LS (r) theory.

Figure 10 illustrates the effect of the fractional parameter β on the dilatation $\breve{e}$ of a hollow sphere, as analyzed using the refined fractional Lord and Shulman (F-LS (r)) theory. The dilatation values range from -6 to 6, indicating both contraction and expansion behaviors depending on the fractional parameter β and the variable r. Three values of β are considered. The curves corresponding to these values show distinct trends in how dilatation $\breve{e}$ varies with r. For $\beta = 0$, the dilatation $\breve{e}$ decreases sharply as r increases from 0.2 to 1. For $\beta = 0.2$, the decrease in dilatation is less pronounced compared to $\beta = 0.5$. For $\beta = 0.5$, the dilatation remains relatively constant or shows minimal variation with r, suggesting a linear or negligible effect when $\beta = 0.5$. The fractional parameter β significantly influences the dilatation $\breve{e}$ behavior. Lower β values lead to more pronounced changes in $\breve{e}$ with respect to r, while higher β values dampen this effect. The refined F-LS (r) theory captures these fractional effects, highlighting its utility in modeling complex material behaviors where fractional calculus is relevant.

Figure 11 illustrates the effect of the fractional parameter β on the radial stress $\breve{\sigma}_r$ of a hollow sphere, as predicted by the refined fractional Lord and Shulman (F-LS (r)) theory. The graph plots the radial stress $\breve{\sigma}_r$ against the parameter r (ranging from 0.2 to 1) for three different values of β: 0.5, 0.2, and 0. The radial stress $\breve{\sigma}_r$ is most compressive (or least tensile) at higher values of r. For $\beta = 0.5$, the radial stress has its maximum positive value (around 3) at $r \approx 0.89$ and its minimum at the inner edge of the hollow sphere. For $\beta = 0.2$, it has its maximum positive value (more than 3) at $r \approx 0.9$ and its minimum at $r \approx 0.45$. For $\beta = 0$, it has its maximum positive value (less than 3) at $r \approx 0.91$ and its minimum at $r \approx 0.39$. The fractional parameter β significantly influences the radial stress $\breve{\sigma}_r$ distribution.

Higher β values lead to more pronounced stress variations, while lower β values result in milder changes.

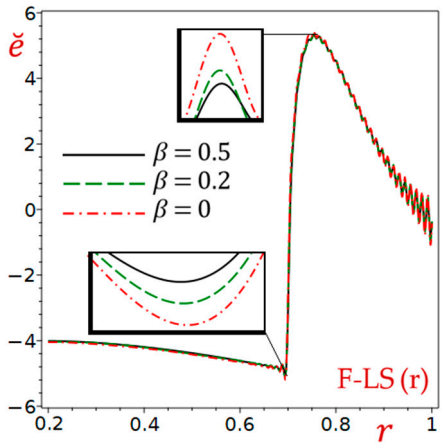


Figure 10. Effect of fractional parameter β on dilatation $\breve{e}$ of the hollow sphere due to the refined F-LS (r) theory.

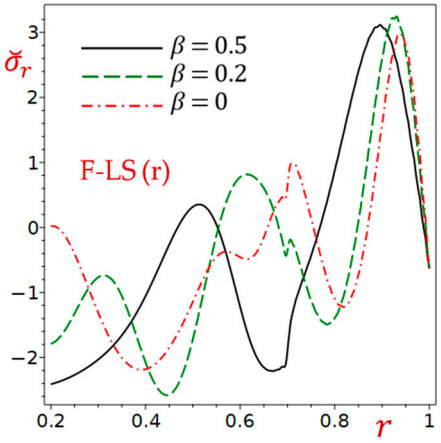


Figure 11. Effect of fractional parameter β on radial stress $\breve{\sigma}_r$ of the hollow sphere due to the refined F-LS (r) theory.

Figure 12 illustrates the effect of the fractional parameter β on the hoop stress $\breve{\sigma}_\theta$ of a hollow sphere based on the refined fractional Lord and Shulman (F-LS (r)) theory. The analysis is based on the refined fractional Lord and Shulman (F-LS (r)) theory, which incorporates fractional calculus to model thermoelastic behavior, providing a more generalized framework than classical or generalized theories. The fractional parameter is given as 0.5 for a specific condition (likely at a reference point or under standard parameters). When $\beta = 0.2$, the hoop stress $\breve{\sigma}_\theta$ is influenced, but the exact value is not explicitly stated in the provided content. The graph or additional context would typically show how $\breve{\sigma}_\theta$ changes compared to the reference value. When $\beta = 0$, the behavior corresponds to a classical or non-fractional model, serving as a baseline for comparison. The graph would likely show a deviation from this baseline as β increases.

As a result, when compared to classical theories, fractional models offer more cautious stress projections. From an engineering perspective, the parameter β is especially important for complex materials with hereditary behavior, such as polymers, biomaterials, porous media, and viscoelastic composites, where the loading history has a significant impact on the current state. However, for simpler homogeneous materials with minor memory effects, classical theories with $\beta = 0$ continue to be sufficient.

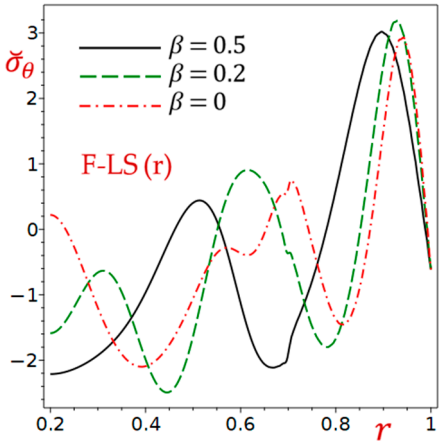


Figure 12. Effect of fractional parameter β on hoop stress $\breve{\sigma}_\theta$ of the hollow sphere due to the refined F-LS (r) theory.

4.3. Effect of Thermal Conductivity Parameter κ_1

Figure 13 compares the effect of the thermal conductivity parameter κ_1 on the temperature $\breve{\Theta}$ of a hollow sphere under two different thermoelastic theories: the refined fractional Lord and Shulman (F-LS (r)) theory and the generalized Lord and Shulman (LS (r)) theory. The plots show curves for four values of κ_1: 1.5, 1.2, 0.9, and 0.6. As κ_1 decreases, the temperature distribution $\breve{\Theta}$ changes, indicating that lower thermal conductivity affects the temperature profile differently in both theories. In Figure 13a the temperature $\breve{\Theta}$ exhibits a non-linear response to changes in r, with the curves showing varying slopes depending on κ_1. Higher κ_1 values (e.g., 1.5) result in steeper temperature gradients, while lower values (e.g., 0.6) lead to flatter distributions. The F-LS (r) theory (with fractional effects) shows smoother and more gradual temperature changes, reflecting the influence of the fractional parameter β. In Figure 13b, the temperature profiles due to LS (r) are more linear compared to the F-LS (r) theory, with distinct separations between curves for different κ_1 values. The impact of κ_1 is more pronounced in this theory, with clear differences in temperature magnitudes across the range of r. The LS (r) theory (without fractional effects) displays sharper distinctions between curves, highlighting the classical thermoelastic behavior.

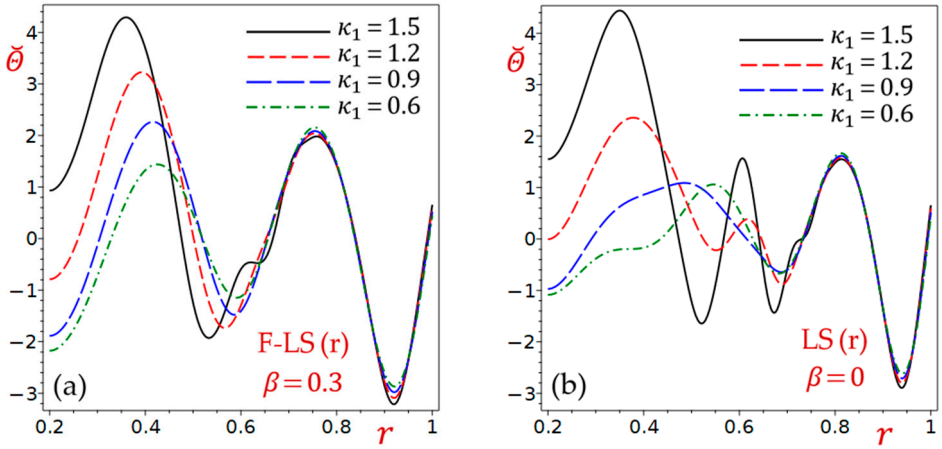


Figure 13. Effect of thermal conductivity parameter κ_1 on the temperature $\breve{\Theta}$ of the hollow sphere due to: (**a**) the refined F-LS (r) and (**b**) the LS (r) theories.

Figure 14 illustrates the effect of the thermal conductivity parameter κ_1 on the radial displacement $\breve{u}$ of a hollow sphere, comparing two different thermoelastic theories. In Figure 14a, the refined fractional Lord–Shulman (F-LS (r)) theory uses a fractional parameter $\beta = 0.3$. The plot shows $\breve{u}$ (radial displacement) against r (radial coordinate). The

displacement becomes more negative (i.e., inward) as r increases, with a sharp decline near $r \approx 0.7$. The refined F-LS (r) theory incorporates fractional calculus ($\beta = 0.3$), leading to a steeper displacement gradient compared to the refined LS (r) theory in Figure 14b. In Figure 14b, the refined generalized Lord and Shulman (LS (r)) theory uses $\beta = 0$ (no fractional effect). The displacement trends vary with κ_1, likely showing how higher conductivity mitigates displacement. As κ_1 decreases (e.g., from 1.5 to 0.6), the displacement $\breve{u}$ becomes less negative, suggesting that lower thermal conductivity reduces inward deformation. The LS (r) theory ($\beta = 0$) shows smoother transitions, emphasizing the fractional model's ability to capture complex thermoelastic interactions.

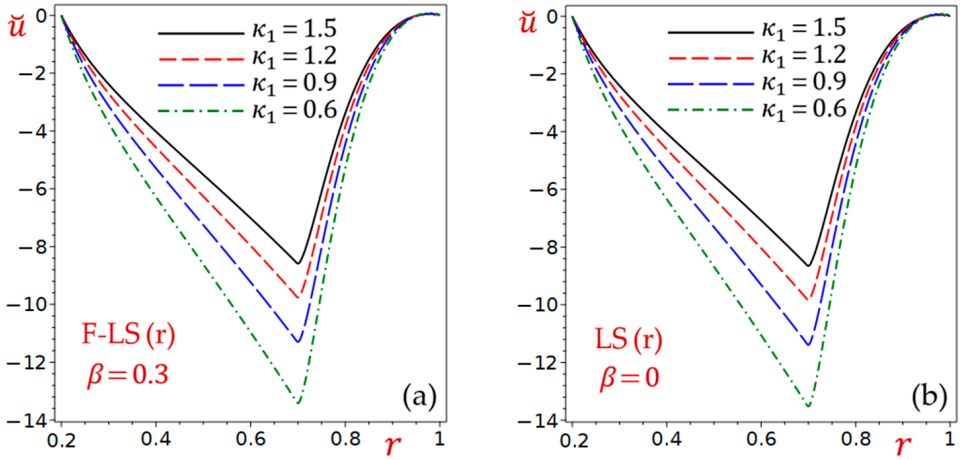


Figure 14. Effect of thermal conductivity parameter κ_1 on the radial displacement $\breve{u}$ of the hollow sphere due to: (**a**) the refined F-LS (r) and (**b**) the LS (r) theories.

The plots in Figure 15 illustrate the effect of the thermal conductivity parameter κ_1 on the dilatation $\breve{e}$ of the hollow sphere under two different thermoelastic theories. In both plots (a) and (b), the dilatation $\breve{e}$ varies with the radial coordinate r, showing a nonlinear distribution across the hollow sphere. The magnitude of $\breve{e}$ decreases as r increases, indicating higher deformation in $0.2 \leq r < 0.7$ and $0.7 < r < 0.85$. For lower values of κ_1 (e.g., $\kappa_1 = 0.6$), the dilatation $\breve{e}$ exhibits larger amplitude (peaks and troughs), suggesting stronger thermoelastic coupling. As κ_1 increases (e.g., $\kappa_1 = 1.5$), the curves become smoother, indicating reduced thermal stress effects.

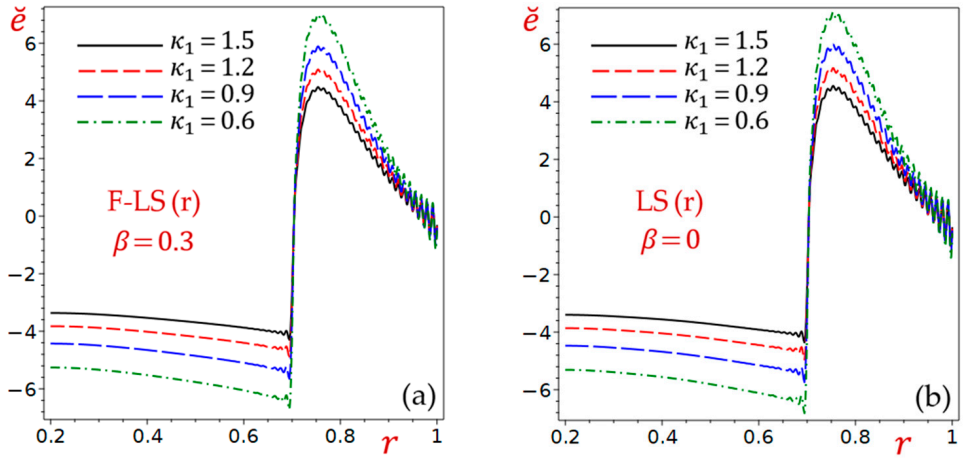


Figure 15. Effect of thermal conductivity parameter κ_1 on the dilatation $\breve{e}$ of the hollow sphere due to: (**a**) the refined F-LS (r) and (**b**) the LS (r) theories.

Figure 16 illustrates the effect of the thermal conductivity parameter κ_1 on the radial stress $\breve{\sigma}_r$ of a hollow sphere under two different thermal theories. In Figure 16a, the refined F-LS (r) theory is used to plot the radial stress $\breve{\sigma}_r$ as a function of r for a fixed fractional parameter $\beta = 0.3$. The stress values are negative, indicating compressive radial stress, and decrease monotonically as r increases from 0.2 to 1. The radial stress $\breve{\sigma}_r$ has a little sensitive to the variation of κ_1 for larger r. In Figure 16b, the radial stress $\breve{\sigma}_r$ is plotted for different values of κ_1 due to the refined LS (r) theory with $\beta = 0$ (no fractional effect). The stress is compressive (negative) and becomes less compressive (closer to zero) as κ_1 decreases. This implies that lower thermal conductivity reduces the magnitude of radial stress. The curves for higher κ_1 (e.g., 1.5) exhibit steeper declines, indicating a stronger dependence of stress on r at higher thermal conductivities. The fractional effect in Figure 16a ($\beta = 0.3$) leads to a distinct stress profile compared to the classical case in (b) ($\beta = 0$), highlighting the influence of fractional calculus on thermoelastic behavior. In Figure 16b, higher κ_1 values result in more pronounced stress variations, suggesting that thermal conductivity significantly impacts stress distribution in the absence of fractional effects. Both theories show compressive radial stress, but the fractional theory (a) may introduce additional nonlinearity or memory effects not captured by the classical theory (b).

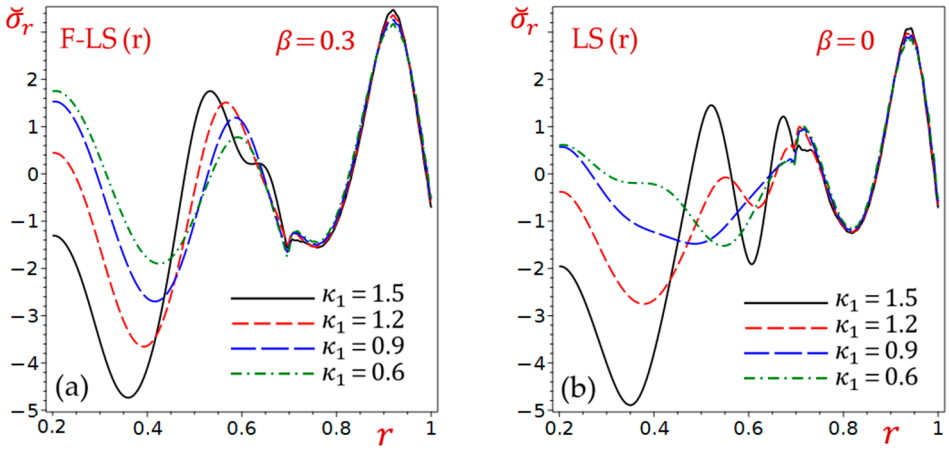


Figure 16. Effect of thermal conductivity parameter κ_1 on the radial stress $\breve{\sigma}_r$ of the hollow sphere due to: (**a**) the refined F-LS (r) and (**b**) the LS (r) theories.

The plots in Figure 17 illustrate the effect of the thermal conductivity parameter κ_1 on the hoop stress $\breve{\sigma}_\theta$ of a hollow sphere under two different thermal theories. In Figure 17a, the hoop stress $\breve{\sigma}_\theta$ is plotted against r for different values of κ_1 by using the refined F-LS (r) theory ($\beta = 0.3$). The hoop stress is compressive (negative) across most of the sphere's thickness, becoming more compressive as r increases. Higher κ_1 values (e.g., 1.5) result in less compressive stress compared to lower κ_1 values (e.g., 0.6). This suggests that increased thermal conductivity reduces the magnitude of hoop stress. In Figure 17b, similar trends are observed, but the stress values are generally less compressive than in fractional cases. The influence of κ_1 follows the same pattern: higher conductivity reduces the stress magnitude. Generally, the fractional parameter β introduces additional stress attenuation, as seen by the more compressive stresses in Figure 17a compared to Figure 17b. Thermal conductivity (κ_1) plays a significant role in stress distribution, with higher conductivity mitigating stress concentration. Both theories predict compressive hoop stresses, but the fractional model ($\beta = 0.3$) predicts higher stress gradients, highlighting the importance of fractional calculus in thermoelastic modeling.

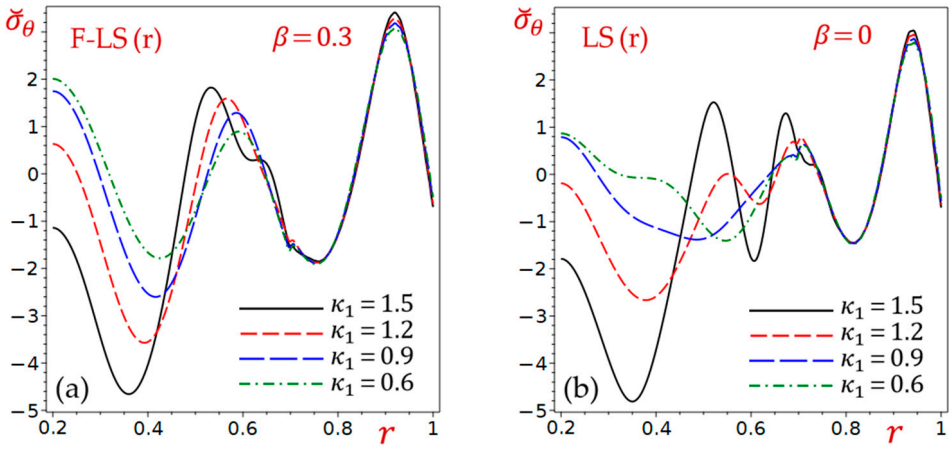


Figure 17. Effect of thermal conductivity parameter κ_1 on the hoop stress $\breve{\sigma}_\theta$ of the hollow sphere due to (**a**) the refined F-LS (r) and (**b**) the LS (r) theories.

4.4. Effect of the Decayed Heat ω

Figure 18 shows the effect of the decayed heat parameter ω on the temperature-mapping $\breve{\vartheta}$ of a hollow sphere under two different thermal theories. Both plots show the temperature-mapping $\breve{\vartheta}$ for ω =15, 13, 11, 9, indicating how the system responds to varying levels of heat decay. Higher ω values likely represent slower heat decay, while lower ω values imply faster decay. In Figure 18a, the F-LS (r) theory incorporates fractional calculus ($\beta = 0.3$), and shows the curves may exhibit smoother transitions or delayed responses due to the fractional derivative. In Figure 18b, the LS (r) theory represents the curves likely to show sharper changes compared to Figure 18b. As ω decreases (faster decay), the temperature distribution $\breve{\vartheta}$ may become more localized or steeper, especially in Figure 18b. The fractional model in Figure 18a with $\beta = 0.3$ likely dampens extreme variations, resulting in more gradual temperature profiles.

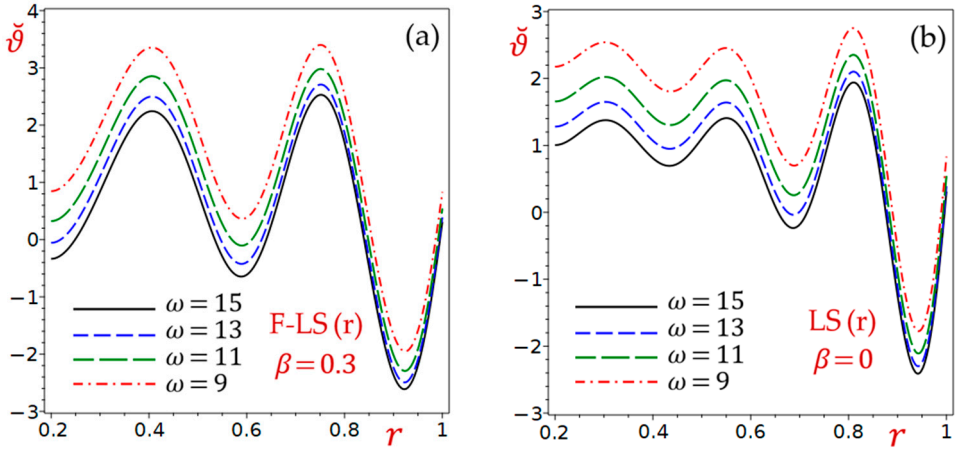


Figure 18. Effect of the decayed heat ω on the temperature-mapping $\breve{\vartheta}$ of the hollow sphere due to: (**a**) the refined F-LS (r) and (**b**) the LS (r) theories.

Figure 19 compares the effect of decayed heat ω on the temperature $\breve{\Theta}$ of a hollow sphere using two different thermal theories. The curves due to F-LS (r) theory in Figure 19a show the temperature distribution $\breve{\Theta}$ for $\omega = 9, 11, 13, 15$ as a function of r (dimensionless radial coordinate). Higher ω values correspond to lower temperatures, indicating that stronger decayed heat effects reduce the temperature more significantly. The fractional parameter $\beta = 0.3$ introduces memory-dependent effects, leading to smoother, more gradual temperature transitions compared to the classical case in Figure 19b. The non-fractional LS (r) theory in Figure 19b shows that the temperature profiles are sharper and

more distinct compared to the fractional case. Similar to Figure 19a, higher ω values reduce the temperature, but the response is more abrupt due to the absence of fractional damping. The fractional model ($\beta = 0.3$) smooths the temperature distribution, reflecting the influence of memory effects in heat conduction. Both theories agree qualitatively (higher $\omega \rightarrow$lower $\breve{\Theta}$), but the fractional parameter β moderates the response, which is critical in materials with anomalous heat diffusion. The plots suggest that $r = 0.6$ to 0.8 is a critical range where temperature differences due to ω are most pronounced.

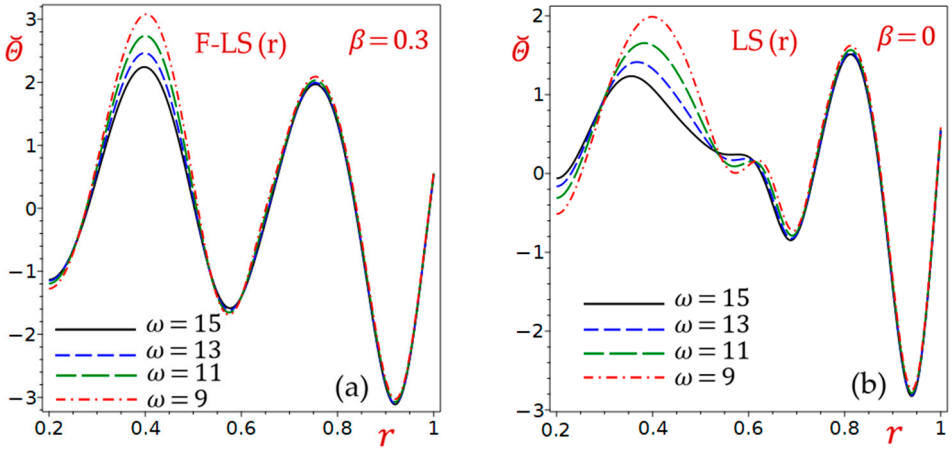


Figure 19. Effect of the decayed heat ω on the temperature $\breve{\Theta}$ of the hollow sphere due to: (**a**) the refined F-LS (r) and (**b**) the LS (r) theories.

Figure 20 compares the effect of the decayed heat parameter ω on the radial displacement $\breve{u}$ of a hollow sphere using two different thermoelastic theories. In Figure 20a, the radial displacement $\breve{u}$ due to F-LS (r) theory becomes more negative (i.e., displacement magnitude increases) as r increases, indicating inward deformation. Higher values of ω (e.g., $\omega = 15$) result in less negative displacement (smaller magnitude), while lower ω (e.g., $\omega = 9$) leads to more pronounced inward displacement. The fractional parameter $\beta = 0.3$ introduces memory-dependent damping, attenuating the displacement response compared to the classical LS theory. Similar trends are observed in Figure 20b, but the radial displacement magnitudes are generally more negative (larger inward deformation) compared to F-LS (r) theory. The absence of fractional damping ($\beta = 0$) makes the system stiffer, amplifying the displacement response to thermal decay (ω). The curves are more sensitive to ω, with $\omega = 9$ causing significantly larger displacements than $\omega = 15$.

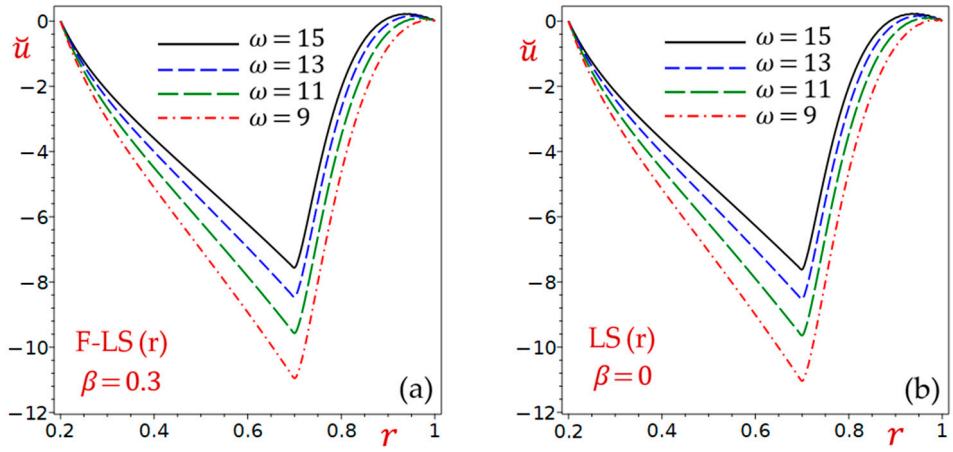


Figure 20. Effect of the decayed heat ω on the radial displacement $\breve{u}$ of the hollow sphere due to: (**a**) the refined F-LS (r) and (**b**) the LS (r) theories.

Figure 21 shows the effect of decayed heat ω on the dilatation $\check{e}$ of a hollow sphere using two different thermoelastic theories. In Figure 21a, the dilatation $\check{e}$ due to F-LS (r) theory, decreases as the decayed heat parameter ω decreases. For higher ω, $\check{e}$ exhibits larger oscillations, while lower ω results in smoother, more damped responses. The fractional parameter $\beta = 0.3$ introduces memory-dependent damping, leading to attenuated dilatation amplitudes compared to the non-fractional case. The absence of fractional effects ($\beta = 0$) in Figure 21b leads to sharper, less damped oscillations in $\check{e}$ across all ω values. Similar to Figure 21a, higher ω values correlate with larger dilatation magnitudes, but the curves are more pronounced due to the lack of fractional damping. The fractional parameter β significantly smooths the dilatation response, reducing peak amplitudes and oscillations. Larger ω values intensify the thermoelastic response, while smaller values ω dampen it, consistent with both theories. The F-LS (r) theory ($\beta = 0.3$) better captures dissipative effects in materials with memory (e.g., viscoelastic solids), whereas the LS (r) theory ($\beta = 0$) suits classical thermoelastic behavior.

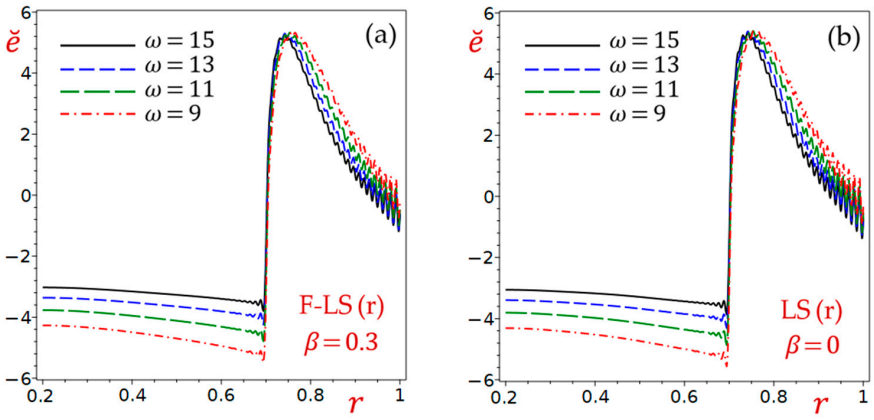


Figure 21. Effect of the decayed heat ω on the dilatation $\check{e}$ of the hollow sphere due to: (**a**) the refined F-LS (r) and (**b**) the LS (r) theories.

In Figure 22, two distinct thermoelastic theories are used to compare the impact of decayed heat ω on the radial stress $\check{\sigma}_r$ in a hollow sphere. The radial stress $\check{\sigma}_r$ caused by F-LS (r) theory, which evolves nonlinearly with the radial coordinate r in Figure 22a, exhibiting noticeable oscillations and amplitude changes as ω lowers. Greater ω leads to steeper gradients and greater stress magnitudes (peaks up to ~3.1). Lower ω smoothes the response and lowers stress amplitudes (peaks close to ~1). With no fractional damping ($\beta = 0$), the radial stress $\check{\sigma}_r$ curves in Figure 22b are smoother and more linear. Although there is less oscillation, higher ω still raises stress magnitudes (e.g., $\omega = 15$ peaks at ~2.9). The reaction is simpler and has a more predictable decay pattern when fractional effects ($\beta = 0$) are absent.

Figure 23 compares two sophisticated thermoelastic theories to show how decaying heat ω affects the hoop stress $\check{\sigma}_\theta$ in a hollow sphere. According to both ideas, the normalized radial coordinate r affects the hoop stress $\check{\sigma}_\theta$. Plotting the stress profiles for various decayed heat values ($\omega = 9, 11, 13, 15$) is done. The amplitude of $\check{\sigma}_\theta$ often decreases as ω increases, suggesting that increased decaying heat lowers the hoop stress. Both explanations support this pattern. Higher ω curves are located underneath lower ω curves. In contrast to the non-fractional model, which shows more abrupt stress fluctuations, the fractional model shows smoother stress variations. This emphasizes how memory and non-local effects are captured by the fractional parameter. The damping effect induced by $\beta = 0.3$ is demonstrated by the significantly decreased peak stress values in Figure 23a compared to Figure 23b. In both models, the stress $\check{\sigma}_\theta$ tends to zero at the outer border ($r \approx 1$), indicating thermally neutral or stress-free conditions at the surface.

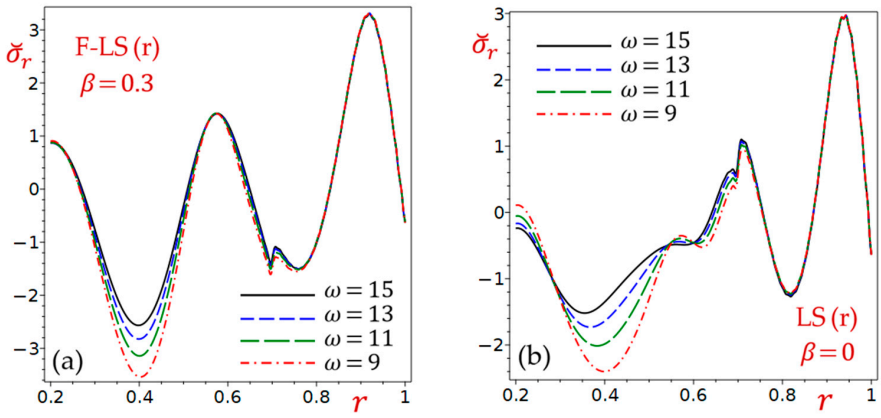


Figure 22. Effect of the decayed heat ω on the radial stress $\breve{\sigma}_r$ of the hollow sphere due to: (**a**) the refined F-LS (r) and (**b**) the LS (r) theories.

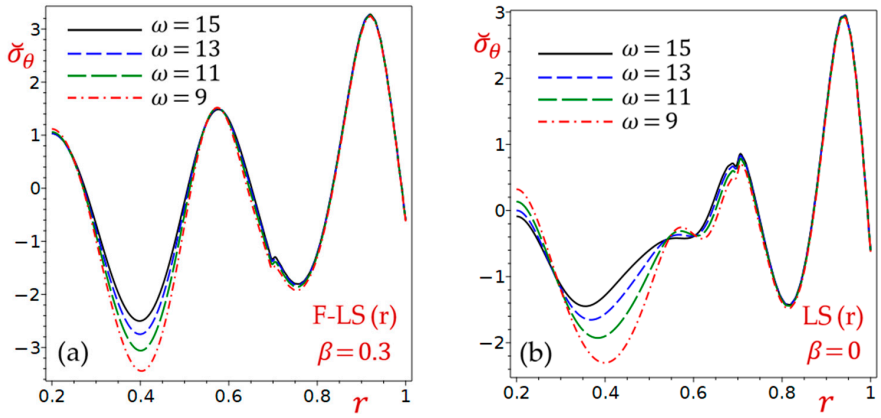


Figure 23. Effect of the decayed heat ω on the hoop stress $\breve{\sigma}_\theta$ of the hollow sphere due to: (**a**) the refined F-LS (r) and (**b**) the LS (r) theories.

5. Conclusions

The study presents a comprehensive analysis of the thermo-fractional behavior of a hollow sphere using various coupled thermoelasticity theories, including Lord–Shulman (LS) theory (simple and refined versions), classical thermoelasticity (CTE) theory, and fractional calculus-based models (F-LS (r), F-LS (s), FD (s)). The governing equations were solved using Laplace transforms and numerical inversion. The key parameters influencing behavior are thermal relaxation time (τ), fractional parameter (β), thermal conductivity (κ_1), and decaying parameter (ω).

- The F-LS (r) theory shows the most dynamic response, capturing complex thermal and mechanical behaviors.
- The classical thermoelasticity (CTE) theory significantly deviates from LS and fractional theories, highlighting differences in fundamental assumptions.
- The simplified fractional models (F-LS (s), FD (s)) underestimate dilatation compared to refined versions.
- The value of $\beta \neq 0$ introduces asymmetry and dynamic responses in temperature-mapping, radial displacement, and stresses.
- The value of $\beta = 0$ leads to more stable and consistent behavior across theories.
- Fractional models exhibit steeper gradients in dilatation and richer stress profiles compared to classical models.
- Fractional models ($\beta \neq 0$) provide more conservative (higher) stress estimates.
- The refined F-LS (r) theory captures smoother stress transitions and nuanced dynamics.

- Higher β increases inward radial displacement.
- Fractional models ($\beta \neq 0$) are better suited for materials with memory effects (e.g., polymers, biomaterials).
- Classical generalized models ($\beta = 0$) suffice for simpler, homogeneous systems.
- Lower κ_1 reduces radial displacement magnitude.
- Higher κ_1 decreases stress magnitudes in both radial and hoop stresses.
- Higher ω (slower decay) mitigates deformation.
- Lower ω (rapid decay) increases thermal stress effects.
- The outer surface ($r \to 1$) experiences greater thermal stress effects.
- The refined F-LS (r) theory offers superior accuracy for complex thermoelastic scenarios.

The choice of thermoelastic theory, fractional parameter (β), and thermal properties (κ_1, ω) critically influences predictions of temperature, deformation, and stress in hollow spheres. Fractional calculus enhances modeling precision for advanced materials, while classical theories remain useful for conventional cases. Engineers should select models based on material behavior and application requirements.

Author Contributions: Conceptualization, A.M.Z. and N.M.S.; methodology, A.M.Z. and M.H.A.; validation, N.M.S., M.H.A. and A.M.Z.; investigation, A.M.Z.; data curation, N.M.S. and M.H.A.; writing—original draft preparation, N.M.S. and M.H.A.; writing—review and editing, A.M.Z.; visualization, N.M.S. and M.H.A.; supervision, A.M.Z.; project administration, A.M.Z.; funding acquisition, A.M.Z. All authors have read and agreed to the published version of the manuscript.

Funding: This project was funded by the Deanship of Scientific Research (DSR) at King Abdulaziz University, Jeddah, Saudi Arabia.

Data Availability Statement: The datasets generated and/or analyzed during the current study are available from the corresponding author on reasonable request.

Acknowledgments: This project was funded by the Deanship of Scientific Research (DSR) at King Abdulaziz University, Jeddah, Saudi Arabia, under grant no. (IPP: 169-130-2025). The authors, therefore, acknowledge DSR with thanks for technical and financial support.

Conflicts of Interest: The authors declared no potential conflicts of interest concerning the research, authorship, and publication of this article.

Nomenclature

α_t	Coefficient of linear thermal expansion
β	Fractional-order parameter ($0 < \beta \leq 1$)
c, κ_1, ϑ_0	Constants
c_v	Specific heat at constant strain
∇^2	Laplacian in spherical coordinates
η	$\equiv \kappa(\Theta)/(\rho c_v)$
e	Volumetric strain (dilatation) $\equiv \nabla \cdot \vec{u}$
e_r, e_θ, e_z	Radial, circumferential (hoop), and axial strains
γ	Thermoelastic coupling parameter $\equiv (3\lambda + 2\mu)\alpha_t$
$\rangle$	An imaginary number unit
$\kappa(\Theta)$	Temperature-dependent thermal conductivity
κ_0	Reference thermal conductivity
λ, μ	Lamé's moduli
M	Sufficiently large integer
ω	An exponent of the decayed heat
Q	Heat source
ρ	Material density of the annular sphere
Re	Real part

σ_r, σ_θ	Radial and circumferential stresses
Θ	Temperature increment $\equiv T - T_0$
τ	First relaxation time
T	Absolute temperature
T_0	Reference temperature
u	Radial displacement
ϑ	Mapped temperature

References

1. Zenkour, A.M.; Abouelregal, A.E. Nonlocal thermoelastic vibrations for variable thermal conductivity nanobeams due to harmonically varying heat. *J. Vibroeng.* **2014**, *16*, 3665–3678.
2. Zenkour, A.M.; Abouelregal, A.E. Effects of phase-lags in a thermoviscoelastic orthotropic continuum with a cylindrical hole and variable thermal conductivity. *Arch. Mech.* **2015**, *67*, 457–475.
3. Mashat, D.S.; Zenkour, A.M.; Abouelregal, A.E. Thermoelastic interactions in a rotating infinite orthotropic elastic body with a cylindrical hole and variable thermal conductivity. *Arch. Mech. Eng.* **2017**, *64*, 481–498. [CrossRef]
4. Abouelregal, A.E.; Zenkour, A.M. Nonlocal thermoelastic semi-infinite medium with variable thermal conductivity due to a laser short-pulse. *J. Comput. Appl. Mech.* **2019**, *50*, 90–98.
5. Ahmed, K.K.; Ahmed, H.M.; Abouelregal, A.E.; Nofal, T.A.; Ismail, M.F. Influence of internal heat source and temperature-dependent effects on thermoelasticity within Lord-Shulman framework using modified extended direct algebraic approach. *J. Therm. Stress.* **2025**, *48*, 1338–1364. [CrossRef]
6. Ramadan, M.E.; Ismail, M.F.; Ahmed, H.M.; Abd-Elmonem, A.; Abdalla, N.S.E.; Ghayad, M.S.; Ahmed, K.K. Exploring the effect of internal heat sources on nonlinear thermoelastic systems via Green–Naghdi theory using contemporary analytical method. *Int. Commun. Heat Mass Transf.* **2025**, *169*, 109867. [CrossRef]
7. Ning, T.-H.; Jiang, X.-Y. Analytical solution for the time-fractional heat conduction equation in spherical coordinate system by the method of variable separation. *Acta Mech. Sin.* **2011**, *27*, 994–1000. [CrossRef]
8. Youssef, H.M.; Abbas, I.A. Fractional order generalized thermoelasticity with variable thermal conductivity. *J. Vibroeng.* **2014**, *16*, 4077–4087.
9. Lotfy, K.; El-Bary, A.A.; Tantawi, R.S. Effects of variable thermal conductivity of a small semiconductor cavity through the fractional order heat-magneto-photothermal theory. *Eur. Phys. J. Plus* **2019**, *134*, 280. [CrossRef]
10. Lotfy, K. Analytical solution of fractional order heat equation under the effects of variable thermal conductivity during photothermal excitation of spherical cavity of semiconductor medium. *Waves Random Complex Media* **2021**, *31*, 239–254. [CrossRef]
11. Geetanjali, G.; Bajpai, A.; Sharma, P.K. Impact of variable thermal conductivity and diffusivity on two temperature fractional thermodiffusive elastic half space with dual phase lags. *Waves Random Complex Media* **2025**, *35*, 4615–4637. [CrossRef]
12. Youssef, H.M. Stat-space approach to three-dimensional thermoelastic half-space based on fractional order heat conduction and variable thermal conductivity under Moor–Gibson–Thompson theorem. *Fractal Fract.* **2025**, *9*, 145. [CrossRef]
13. Hendy, M.H.; Ezzat, M.A. Fractional piezoelectric thermo-viscoelastic materials with variable properties. *J. Therm. Stress.* **2025**, *48*, 441–457. [CrossRef]
14. Ma, Y.; He, T. The transient response of a functionally graded piezoelectric rod subjected to a moving heat source under fractional order theory of thermoelasticity. *Mech. Adv. Mater. Struct.* **2017**, *24*, 789–796. [CrossRef]
15. Bhoyar, S.; Varghese, V.; Khalsa, L. An exact analytical solution for fractional-order thermoelasticity in a multi-stacked elliptic plate. *J. Therm. Stress.* **2020**, *43*, 762–783. [CrossRef]
16. Tian, L.; Peng, W.; He, T. A modified fractional-order thermo-viscoelastic model and its application in thermal-induced nonlocal response analysis of a microscale plate. *Arch. Appl. Mech.* **2023**, *93*, 687–705. [CrossRef]
17. Roy, S.; Lahiri, A. Fractional order thermoelastic model with voids in three-phase-lag thermoelasticity. *Comput. Sci. Math. Forum* **2023**, *7*, 57.
18. Povstenko, Y.; Klekot, J. Fractional heat conduction with heat absorption in a sphere under Dirichlet boundary condition. *Comput. Appl. Math.* **2018**, *37*, 4475–4483. [CrossRef]
19. Mittal, G.; Kulkarni, V.S. Two temperature fractional order thermoelasticity theory in a spherical domain. *J. Therm. Stress.* **2019**, *42*, 1136–1152. [CrossRef]
20. Shah, N.A.; Ameer Ahammad, N.; Vieruc, D.; Yook, S.-J.; Alrabaiah, H. Analytical solutions for time-fractional diffusion equation with heat absorption in spherical domains. *Ain Shams Eng. J.* **2023**, *14*, 102031. [CrossRef]
21. Sheikh, S.; Khalsa, L.; Makkad, G.; Varghese, V. Fractional dual-phase-lag hygrothermoelastic model for a sphere subjected to heat-moisture load. *Arch. Appl. Mech.* **2024**, *94*, 1379–1396. [CrossRef]

22. Kanoria, M.; Ghosh, M.K. Study of dynamic response in a functionally graded spherically isotropic hollow sphere with temperature dependent elastic parameters. *J. Therm. Stress.* **2010**, *33*, 459–484. [CrossRef]
23. Abo-Dahab, S.M.; Abbas, I.A. LS model on thermal shock problem of generalized magneto-thermoelasticity for an infinitely long annular cylinder with variable thermal conductivity. *Appl. Math. Model.* **2011**, *35*, 3759–3768. [CrossRef]
24. Sur, A.; Kanoria, M. Fractional order two-temperature thermoelasticity with finite wave speed. *Acta Mech.* **2012**, *223*, 2685–2701. [CrossRef]
25. Islam, M.; Kanoria, M. One-dimensional problem of a fractional order two-temperature generalized thermo-piezoelasticity. *Math. Mech. Solids* **2013**, *19*, 672–693. [CrossRef]
26. Shariyat, M.; Sedaghat, A.M. Nonlinear finite-speed thermoelasticity with physically possible fractional orders for wave propagation, reflection, and mixing analyses in annular discs with initial rotational pre-deformations. *Acta Mech.* **2022**, *233*, 725–752. [CrossRef]
27. Shariyat, M.; Sedaghat, A.M. Generalized fractional-order hygro-thermo-viscoelastic wave propagation/reflection in annular spinning discs: Comparisons with the classical and Lord–Shulman thermo-viscoelastic models. *J. Braz. Soc. Mech. Sci. Eng.* **2023**, *45*, 506. [CrossRef]
28. Zenkour, A.M.; Saeed, T.; Al-Raezah, A.A. Fractional order of refined Lord–Shulman model for a 1D thermoelastic response of skin tissue due to ramp-type heating. *Arch. Appl. Mech.* **2024**, *94*, 989–1003. [CrossRef]
29. Babaei, M.H.; Chen, Z.T. Hyperbolic heat conduction in a functionally graded hollow sphere. *Int. J. Thermophys.* **2008**, *29*, 1457–1469. [CrossRef]
30. Zenkour, A.M.; Abouelregal, A.E.; Alnefaie, K.A.; Zhang, X.; Aifantis, E.C. Nonlocal thermoelasticity theory for thermal-shock nanobeams with temperature-dependent thermal conductivity. *J. Therm. Stress.* **2015**, *38*, 1049–1067. [CrossRef]
31. Abbas, I.A. Analytical solution for a free vibration of a thermoelastic hollow sphere. *Mech. Based Des. Struct. Mach.* **2015**, *43*, 265–276. [CrossRef]
32. Mishra, K.C.; Sharma, P.K. Radial vibrations of functionally graded spheres due to thermal load. *J. Therm. Stress.* **2020**, *43*, 1531–1546. [CrossRef]
33. Jani, S.M.H.; Kiani, Y.; Tadi Beni, Y. Generalized piezothermoelasticity of hollow spheres under thermal shock using Lord–Shulman theory. *J. Therm. Stress.* **2024**, *47*, 347–362. [CrossRef]
34. Branco, J.F.; Pinho, C.T.; Figueiredo, R.A. Heat conduction in the hollow sphere with a power-law variation of the external heat transfer coefficient. *Int. Commun. Heat Mass Transf.* **2000**, *27*, 1067–1076. [CrossRef]
35. Kar, A.; Kanoria, M. Generalized thermoelasticity problem of a hollow sphere under thermal shock. *Eur. J. Pure Appl. Math.* **2009**, *2*, 125–146.
36. Ghosh, M.K.; Kanoria, M. Analysis of thermoelastic response in a functionally graded spherically isotropic hollow sphere based on Green–Lindsay theory. *Acta Mech.* **2009**, *207*, 51–67. [CrossRef]
37. Sharma, D.K.; Thakur, P.C.; Sarkar, N. Effect of dual-phase-lag model on free vibrations of isotropic homogenous nonlocal thermoelastic hollow sphere with voids. *Mech. Based Des. Struct. Mach.* **2022**, *50*, 3949–3965. [CrossRef]
38. Sharma, D.K.; Sharma, A.; Mondal, S.; Bachher, M. Transient thermo-diffusive responses in a nonlocal elastic sphere due to harmonically varying heat sources. *Int. J. Geomath.* **2023**, *14*, 6. [CrossRef]
39. Lord, H.W.; Shulman, Y.A. A generalized dynamical theory of thermoelasticity. *J. Mech. Phys. Solids* **1967**, *15*, 299–309. [CrossRef]
40. Sobhy, M.; Zenkour, A.M. Refined Lord–Shulman theory for 1D response of skin tissue under ramp-type heat. *Materials* **2022**, *15*, 6292. [CrossRef]
41. Aljadani, M.H.; Zenkour, A.M. Effect of magnetic field on a thermoviscoelastic body via a refined two-temperature Lord–Shulman model. *Case Stud. Therm. Eng.* **2023**, *49*, 103197. [CrossRef]
42. Alghamdi, A.A.; Zenkour, A.M. Refined one relaxation time-fractional theory for the thermoelastic response of circular cylinders with variable thermal conductivity. *Mathematics* **2025**, *13*, 3497. [CrossRef]
43. Hafed, Z.S.; Zenkour, A.M. Thermal shock of anisotropic hollow cylinders via one relaxation time-fractional model. *Acta Mech.* **2026**, *237*, 2133–2150. [CrossRef]
44. Aljadani, M.H.; El-Mekawy, H.F.; Hafed, Z.S.; Zenkour, A.M. Nonlocal magneto-thermoelastic interactions in a thin slim strip due to a moving heat source via a refined Lord–Shulman theory. *J. Comput. Appl. Mech.* **2025**, *56*, 345–363.
45. Hafed, Z.S.; Zenkour, A.M. Thermal shock of a two-layer solid based on the refined Lord–Shulman model. *Mech. Adv. Mater. Struct.* 2026, *in press*. [CrossRef]
46. Dubner, H.; Abate, J. Numerical inversion of Laplace transforms by relating them to the finite Fourier cosine transform. *J. ACM* **1968**, *15*, 115–123. [CrossRef]

Disclaimer/Publisher's Note: The statements, opinions and data contained in all publications are solely those of the individual author(s) and contributor(s) and not of MDPI and/or the editor(s). MDPI and/or the editor(s) disclaim responsibility for any injury to people or property resulting from any ideas, methods, instructions or products referred to in the content.